QUANTUM MECHANICS

In search of multipath interference using large molecules

Joseph P. Cotter,[1]*† Christian Brand,[1] Christian Knobloch,[1] Yigal Lilach,[2] Ori Cheshnovsky,[2,3] Markus Arndt[1]

The superposition principle is fundamental to the quantum description of both light and matter. Recently, a number of experiments have sought to directly test this principle using coherent light, single photons, and nuclear spin states. We extend these experiments to massive particles for the first time. We compare the interference patterns arising from a beam of large dye molecules diffracting at single, double, and triple slit material masks to place limits on any high-order, or multipath, contributions. We observe an upper bound of less than one particle in a hundred deviating from the expectations of quantum mechanics over a broad range of transverse momenta and de Broglie wavelength.

INTRODUCTION

Many quantum technologies rely on the ability to prepare and manipulate the wave function ψ of a quantum object. For most applications, the advantage of quantum systems over their classical counterparts stems from the superposition principle—quantum states can be coherently split, simultaneously exploring larger regions of phase-space as they evolve than allowed classically. Typically, the information of interest is encoded in the relative phase difference between superpositions of quantum degrees of freedom, such as energy, spin, momentum, or position. In practice, this phase difference is measured by recombining the superposition states to form an interferometer. Examples include atomic clocks (*1*), quantum processing devices (*2*, *3*), magnetic sensors (*4*), and matter-wave interferometers using atoms (*5*, *6*) and macromolecules (*7*).

The interpretation of the wave function continues to intrigue both theorists (*8*–*11*) and experimentalists (*12*, *13*). Although it is not directly observable, it can be inferred from measurements of the probability density P using Born's rule

$$P = |\psi|^2 \quad (1)$$

As long as the underlying quantum dynamics are linear, Eq. 1 can be derived from decision theory (*14*), entanglement (*15*), or measurements confined to closed Hilbert spaces (*16*). However, nonlinear extensions to quantum mechanics for massive objects (*17*–*23*), which are stimulated by the apparent absence of quantum phenomena in macroscopic systems, can, in principle, result in modifications to Born's rule (*24*). This is somewhat akin to the breakdown of the superposition principle in nonlinear optics. Although some nonlinear extensions to quantum mechanics (*25*, *26*) have been ruled out (*27*) or constrained by experiment (*28*), recent advances (*29*) in probing quantum phenomena in systems of increasing mass (*30*–*32*) or larger state separation (*33*) motivate further experimental exploration.

Sorkin (*34*) showed that the quadratic form of Born's rule implies that no matter how many paths are accessible to a quantum object in configuration space, the probability of a particular outcome can always be decomposed into a series of terms containing at most two of the allowed paths. This insight has guided a number of recent experiments searching for multipath interference using coherent light and single photons (*35*–*38*), light carrying orbital angular momentum (*39*), and molecular spins in nuclear magnetic resonance experiments (*40*). Here, we compare the interference patterns created by free-flying macromolecules behind single, double, and triple slits, providing an explicit test of multipath interference for the center-of-mass wave function of massive quanta.

RESULTS

Figure 1A shows the experimental layout. A vacuum window coated with a thin, homogeneous layer of phthalocyanine (PcH_2) provides a source of molecules with a mass M = 515 atomic mass unit (amu). A tightly focused laser beam desorbs them, producing a molecular beam along z with a mean velocity v = 240 m/s and a full width at half maximum Δv = 130 m/s. This corresponds to de Broglie wavelengths in the range of about λ_{dB} = 2.5 to 5.0 pm. After propagating a distance L_1 = 1.55 m under high vacuum, the molecules impinge on a 25-nm–thick amorphous carbon mask containing a vertical array of one single, two double, and triple slits. The slits have an average transverse opening width of a = 80 nm. The double slits have periodicities d = 100 and 200 nm, and the triple slit has a periodicity of d = 100 nm. Figure 2 shows a transmission electron microscopy (TEM) image of a part of the triple slit (see Materials and Methods and the Supplementary Materials). The slits are arranged vertically above one another on the same substrate and are exposed to the molecular beam simultaneously.

In this experiment, the transverse coherence length of the molecular beam at the mask $2\lambda_{dB}L_1/\Delta x$ is limited by the size of the molecular source [Δx = 1.6(1) μm] and ranges from 5 to 10 μm. This exceeds the maximum transverse separation between slits in each mask by more than an order of magnitude. Behind the mask, the molecules propagate a further distance L_2 = 0.58 m before they are adsorbed on a quartz plate where they are imaged using laser-induced fluorescence.

Consider the three idealized slits illustrated in Fig. 1B. If the spatial coherence of a molecular beam encountering these apertures extends over all three slits, the final wave function is described by the coherent sum of the individual wave functions transiting each slit

$$\psi_{ABC} = \psi_A + \psi_B + \psi_C \quad (2)$$

[1]Faculty of Physics, Vienna Center for Quantum Science and Technology, University of Vienna, Boltzmanngasse 5, A-1090 Vienna, Austria. [2]Center for Nanoscience and Nanotechnology, Tel Aviv University, 69978 Tel Aviv, Israel. [3]School of Chemistry, Raymond and Beverly Faculty of Exact Sciences, Tel Aviv University, 69978 Tel Aviv, Israel.
*Present address: Centre for Cold Matter, The Blackett Laboratory, Imperial College London, London SW7 2BW, UK.
†Corresponding author. Email: j.cotter@imperial.ac.uk

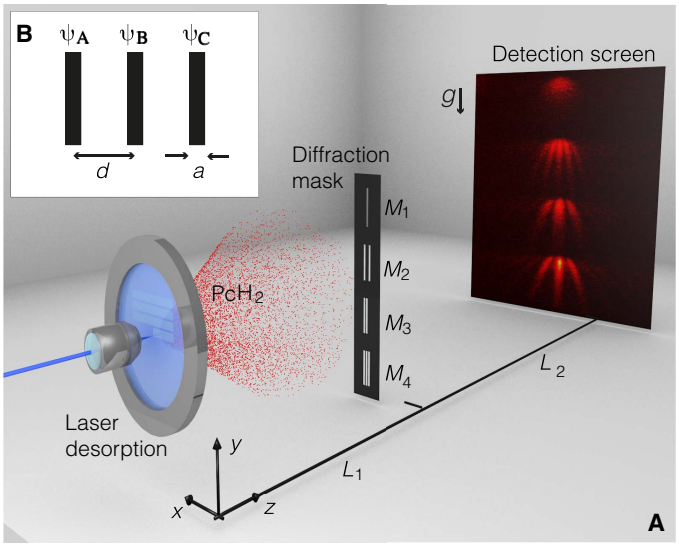

Fig. 1. Experimental setup. (**A**) Focused laser source produces a thermal beam of PcH_2 molecules, which diffracts at a vertical array of single, double, and triple slits, which are aligned to the local gravitation field *g*, before landing on a thin quartz detection screen. The deposited molecules are observed using high-resolution fluorescence imaging. (**B**) Schematic of the triple slit. The openings (black) have a transverse width a = 80 nm, and their centers are separated by a distance d = 100 nm.

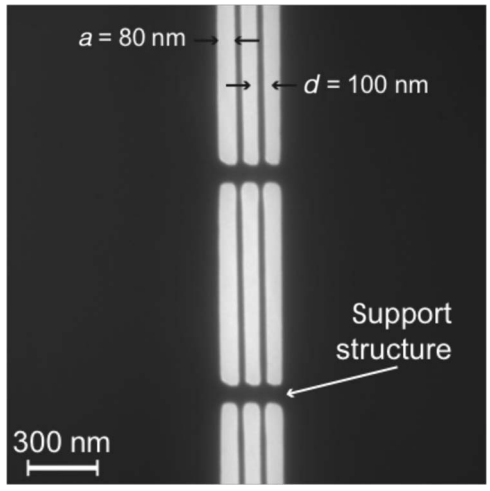

Fig. 2. Diffraction mask. TEM image of a part of the M_4 submask of the triple slit. The openings in the mask (white) are a = 80 nm wide and have a period of d = 100 nm.

This results in a probability density $P_{ABC} = |\psi_{ABC}| = |\psi_A + \psi_B + \psi_C|^2$, which can be written in terms of one- and two-path interference contributions only as

$$P'_{ABC} = (P_{AB} + P_{AC} + P_{BC}) - (P_A + P_B + P_C) \quad (3)$$

Here, P'_{ABC} represents the probability density expected, according to Born's rule, when all three paths are available. P_{AB} is the measured probability density when only paths A and B are open, P_A applies when only path A is open, and so on. By comparing measured three-path interference patterns with a combination of one- and two-path patterns, one can therefore provide an upper bound to the contribution of multipath interference using Sorkin's criterion (*34*) through a nonzero measurement of the dimensionless parameter

$$\varepsilon(x, \lambda_{dB}) = P_{ABC} - P'_{ABC}$$
$$= P_{ABC} - (P_{AB} + P_{AC} + P_{BC}) + (P_A + P_B + P_C) \quad (4)$$

Here, x is the transverse position on the detection screen and λ_{dB} is the de Broglie wavelength of the interfering quanta.

Within an experimental run, we deposit about 2×10^4 molecules in an area of the detection screen measuring $80 \times 280\ \mu m^2$. This number density is sufficiently dilute, even in the densest regions, that N_γ, the number of fluorescence photons detected, remains proportional to the number of molecules in a given region, $N = \alpha N_\gamma$.

According to Eq. 4, seven different interference patterns are required to place bounds on $\varepsilon(x, \lambda_{dB})$. However, in this experiment, the interference patterns P_{AB} and P_{BC} are expected to differ only by a translation of 100 nm along x. This is two orders of magnitude smaller than the spatial separation of the diffraction fringes and below the limit of our spatial resolution. We can therefore simplify Eq. 4 as

$$\varepsilon(x, \lambda_{dB}) = N_3^{(a,d)}(x, \lambda_{dB}) - 2N_2^{(a,d)}(x, \lambda_{dB}) -$$
$$N_2^{(a,2d)}(x, \lambda_{dB}) + 3N_1^{(a)}(x, \lambda_{dB}) \quad (5)$$

Here, N is the number of molecules, subscripts label the number of paths available, and superscripts denote the respective slit width and separation. This simplification is valid because $N_A \approx N_B \approx N_C = N_1^{(a)}$, $N_{AB} \approx N_{BC} = N_2^{(a,d)}$, $N_{AC} = N_2^{(a,2d)}$, and $N_{ABC} = N_3^{(a,d)}$. This allows only four submasks to be used: M_1 with a single slit, M_2 with two slits separated by d, M_3 with two slits separated by $2d$, and M_4 with three slits separated by d.

Figure 3 (A to D) shows typical fluorescence images for molecules diffracted at submasks M_1 to M_4 in a region of $80 \times 280\ \mu m^2$. This region was chosen to be slightly larger than the single-slit diffraction pattern, which sets the natural length scale for these experiments. In all images, we observe a broad transverse distribution of molecules, consistent with a single-slit diffraction envelope. However, where more than one path is available, additional fringes, consistent with $\lambda_{dB} = xd/L_2$, are observed. Here, m is an integer labeling the diffraction order, and we have made the small-angle approximation $\sin(\theta) \approx \theta \approx x/L_2$. Slower molecules have more time to fall as they travel from the source to the screen, resulting in larger separations between diffraction orders than those of faster particles. The molecular velocity, and therefore the de Broglie wavelength, is encoded in the vertical position of molecules on the detection screen. Hence, we are able to post-select molecules with different de Broglie wavelengths after each experiment. Figure 3E shows the corresponding value of $\varepsilon(x, \lambda_{dB})$ for the interference patterns shown in Fig. 3 (A to D) after subtraction in accordance with Eq. 5. We see that the deviation from zero is typically at the one-molecule level or fewer.

To compare results from different experimental runs as well as our values to earlier measurements with photons (*35*, *37*, *40*), we rescale

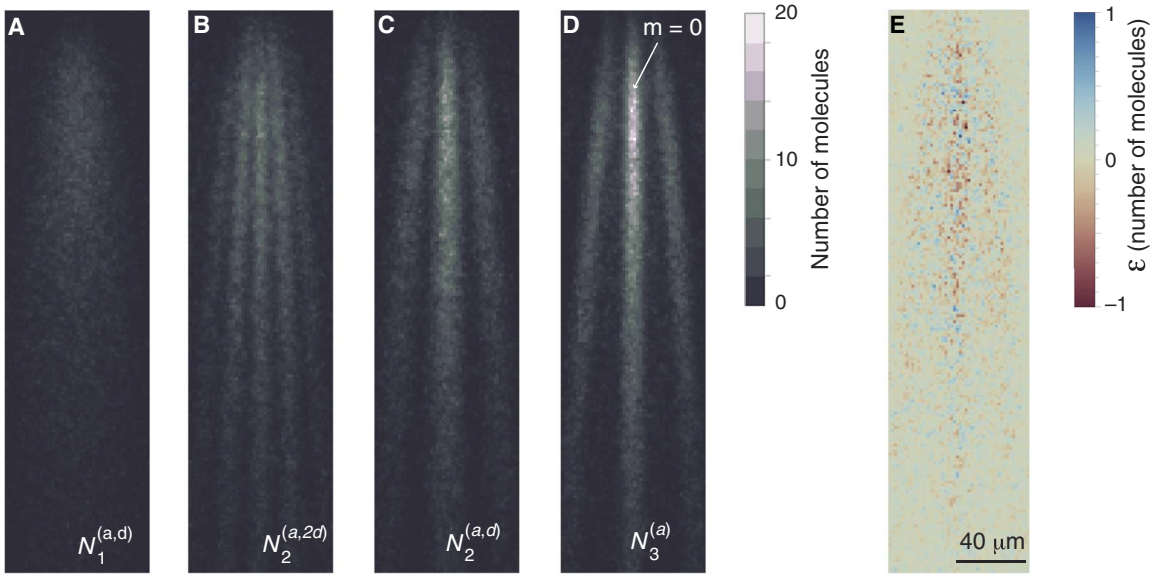

Fig. 3. Molecule diffraction patterns. Fluorescence images of molecules after diffraction at (**A**) a single slit, (**B**) a double slit with period 2*d*, (**C**) a double slit with period *d*, and (**D**) a triple slit with period *d*. Slower molecules fall further under gravity in the time it takes them to reach the screen. This results in a larger separation between diffraction orders further down the screen. All images are aligned vertically with respect to gravity. In (D), we have highlighted the center of the $m = 0$ fringe. (**E**) Sorkin parameter $\varepsilon(x, \lambda_{dB})$ for the interference patterns (A to D) calculated in accordance with Eq. 5.

$\varepsilon(x, \lambda_{dB})$ by the total number of molecules detected for each de Broglie wavelength, $N_{total}(\lambda_{dB})$, within the triple-slit interference pattern

$$\kappa(x, \lambda_{dB}) = \frac{\varepsilon(x, \lambda_{dB})}{N_{total}(\lambda_{dB})} \quad (6)$$

This ratio compares the number of molecules that deviate from the predictions of quantum mechanics to the total number of molecules detected for a given de Broglie wavelength and therefore provides a measure of any potential violation that is independent of the particle flux and integration time. Note that the precise definition of κ varies throughout the existing literature. In many cases, it is the intensity of particles detected at the center of the interference pattern that is used. However, in far-field molecule interferometry, the interaction energy between the interfering particles and the diffractive element can alter the relative intensity of each diffraction order, resulting in species- and diffraction-dependent values of κ. In contrast, the total number of molecules detected remains independent of the diffraction process at low energies.

Figure 4A shows the normalized Sorkin parameter $\kappa(x, \lambda_{dB})$ averaged over five experimental runs, each of which takes about 8 hours to accumulate. We see that any residual structure remaining in $\varepsilon(x, \lambda_{dB})$ from Fig. 3E is greatly reduced by the combined action of averaging and normalizing to the total number of molecules detected. To produce this figure, we have combined the four interference patterns of Fig. 3 (A to D) in accordance with Eqs. 4 to 6. The absence of pronounced peaks qualitatively constrains multipath contributions to the interference patterns generated in our molecule interferometer.

In a single measurement, we obtain interference patterns for particles with de Broglie wavelengths spanning more than an entire octave as well as a broad range of transverse positions. More details relating to the conversion of vertical position on the charge-coupled device (CCD) camera to de Broglie wavelength can be found in Materials and Methods and the Supplementary Materials. To quantitatively constrain multipath interference, we focus on κ recorded at the center of the zeroth diffraction fringe and a transverse slice with a de Broglie wavelength of 3.5 pm. Figure 4 (B and C) shows $\kappa(0, \lambda_{dB})$ and $\kappa(x, 3.5\ \text{pm})$ averaged over five experimental runs. The black line depicts the mean value, with the shaded region illustrating the accompanying 1σ SE. We see no significant deviation of κ from zero beyond our statistical uncertainty across the entire range of de Broglie wavelengths or transverse momenta probed.

DISCUSSION

Our molecular experiment provides a direct constraint on contributions to multipath interference using massive particles by comparing the interference patterns resulting from single-, double-, and triple-slit experiments. Matter waves have a different dispersion relation than light, which has enabled us to place bounds on multipath interference across a range of de Broglie wavelengths spanning more than an octave, in addition to a broad range of transverse momenta, in a single experimental run.

We observe that, on average, less than one molecule in a hundred deviates from the coherent, Schrödinger description of quantum mechanics when compared with the corresponding local number of molecules of the same de Broglie wavelength in a triple-slit experiment. This results in an upper limit of $|\kappa|^2 \leq 10^{-2}$ across de Broglie wavelengths ranging from 2.5 to 5.0 pm and transverse positions ranging over 80 μm centered on the zeroth interference fringe.

Unlike photons, which are detected destructively, here, the interfering quanta are durable molecules that stick to a screen where they can be detected in a nondestructive manner, even days after deposition (*41*). Whether the wavelike description of quantum objects extends to higher masses (*29*, *42*) remains an open question that motivates further experiments using larger, more massive, and complex particles. However, the long integration time required to produce a single-molecule

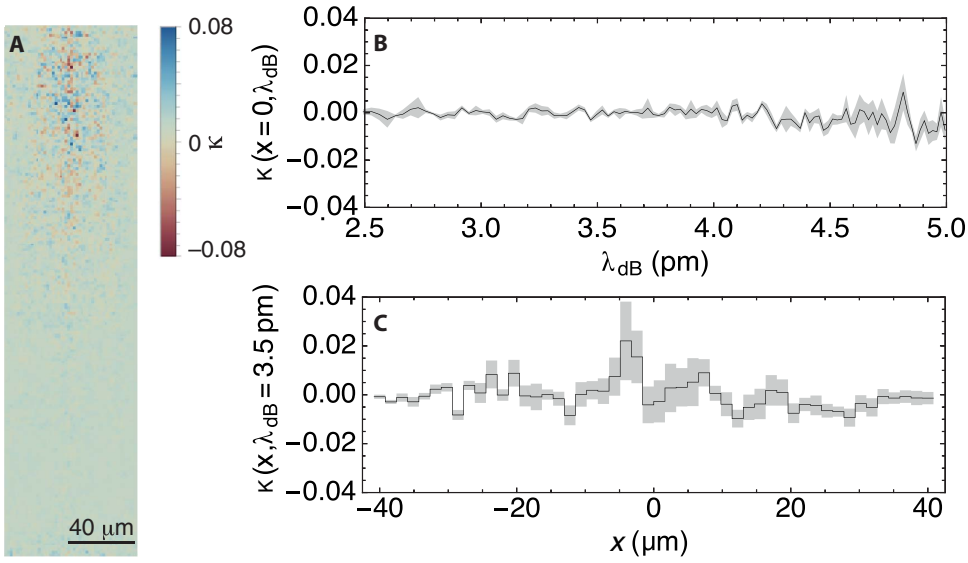

Fig. 4. Bounding multipath interference. (**A**) Normalized Sorkin parameter $\kappa(x, \lambda_{dB})$. (**B**) $\kappa(0, \lambda_{dB})$, the normalized Sorkin parameter as a function of de Broglie wavelength at the center of the $m = 0$ interference fringe. (**C**) $\kappa(x, 3.5\ \text{pm})$, the normalized Sorkin parameter as a function of transverse position on the detection screen for a mean de Broglie wavelength of 3.5 pm. Each figure shows the average over five different experimental runs. In (B) and (C), black lines show the mean, whereas shaded gray areas enclose the 1σ SE. The spatial resolution in all figures is limited by the point-spread function of the imaging system, which is 1.6 μm, approximately four pixels in the plane of the molecular detection screen.

interference pattern limits our statistics, which are the dominant uncertainty in this experiment. Further progress hinges on the development of new sources for slow, cold, and collimated macromolecular, cluster, or nanoparticle beams.

Direct tests of multipath interference using beams of molecules are best implemented in a single diffraction grating scheme, such as the one used in our present work. State-of-the-art material diffraction gratings have already reached their natural size limit, with masks as thin as a single atomic layer (*43*); further advances may therefore require optical gratings or new methods of producing effective slits for matter waves.

High-order interference terms, resulting in finite values of κ, are predicted by quantum mechanics. These additional terms can be understood using the Feynman path integral approach, wherein nonlinear paths also add up constructively to contribute to the final interference pattern (*44*, *45*). For a triple-slit experiment, such as the one presented here, the maximum value of this multipath contribution scales as $\lambda_{dB}^{3/2}/(a\,d^{1/2})$. The relatively high mass of our interfering quanta, which are derived from a thermal source, results in a short de Broglie wavelength. This suppresses the multipath contribution to the interference patterns well below our current precision. However, matter-wave interferometry using cold, low-mass atoms, such as helium or lithium, can achieve very long de Broglie wavelengths and may be able to reach the necessary precision.

MATERIALS AND METHODS

Experimental design

The experiment is housed in a 2.14-m-long vacuum chamber with a background pressure below 10^{-7} mbar (*41*). At this pressure, collisions with background gas can be safely neglected. Furthermore, collisions predominantly prevent the molecules from reaching the small detection region, whereby they reduce the count rate without affecting the shape of the diffraction patterns. Each experimental run took about 8 hours. Approximately 50 mg of PcH_2 ($M = 515$ amu) was evaporated onto a CF100 vacuum window, resulting in a homogeneous layer, only a few micrometers thick (*41*). Evaporating molecules from the coated window using a tightly focused 60-mW laser beam with a wavelength of 421 nm produced a dilute molecular beam along z, with, on average, less than one molecule passing through the grating at any given time. Particles leave the surface from a circular spot with a diameter of $\Delta x = 1.6(1)$ μm, measured using an optical microscope. The beam was replenished in situ by translating the window laterally to expose new regions of the surface to the laser beam. This ensures that the position of the beam relative to the diffraction mask remains fixed. After desorption, the molecules propagate a distance of $L_1 = 1.55$ m before coherently illuminating the diffraction mask consisting of four sets of slits (M_1 to M_4). The angular spread of the molecular beam is well described by a cosine distribution, resulting in a flux of particles varying by $<10^{-6}$ across the 0.6-mrad solid angle required to simultaneously illuminate all slits. The mask was positioned relative to the molecular beam with a precision of 25 μm using an *xy* translation stage, and the slits were orientated with respect to gravity (*y* axis) to better than a few milliradians.

After passing through, the mask molecules arrive at a quartz plate where they stick. The molecular diffraction patterns were then revealed by illuminating the quartz plate using a 661-nm laser and observing the resulting fluorescence from the deposited molecules. The illumination laser beam has a top-hat intensity distribution produced by reflecting a Gaussian beam from the surface of a spatial light modulator (SLM) before passing through a rotating ground-glass diffuser. Each interference pattern was imaged using a 20-s exposure, during which the SLM cycled through 100 different interference masks, averaging over the laser beam phase fronts, resulting in an average intensity that varies by a few percent over the entire region of interest. Fluorescence photons were collected using a 20× objective (Zeiss Ultrafluar), which focuses them onto an electron-multiplying CCD camera (Andor iXon 885-KCSVP) containing 1003 pixels × 1004 pixels with an area of 8 × 8 μm^2 each. The

point spread function of the imaging system is about four times larger than the size of a single pixel and limits our spatial resolution. We therefore averaged the two-dimensional (2D) interferograms over blocks of 4 pixels × 4 pixels.

Fluorescence photons were separated from the illumination light using a 711-nm band-pass filter with a bandwidth of 25 nm and an optical density of >7. Special care is taken to avoid saturation and nonlinear effects by having only thin layers of molecules deposited. On average, each molecule contributes 1800 CCD counts (more details are described in the Supplementary Materials).

Diffraction mask

The mask was fabricated into a 25-nm-thick amorphous carbon membrane (Ted Pella). The slits were machined using a focused gallium ion beam (Raith ionLine) with a kinetic energy of 35 kV, a one-dimensional (1D) beam density of 48×10^3 pC/m, a current of 19.2 pA, and a dwell time of 0.72 ms. During the writing process, the ion beam was translated across the substrate in steps of 1 nm. The focused waist of the ion beam is about 60 nm, requiring each individual subslit to be exposed twice to realize a slit width of 80 nm.

The morphology of the mask was investigated using TEM. The mask extends over a height (y axis) of 958 μm and consists of four submasks: M_1 containing a single slit, M_2 and M_3 containing double slits, and M_4 containing a triple slit. Each slit is 21 μm long and consists of a vertical array of 19 subslits, separated from one another by 92(5)-μm-long -support bars, which stabilize the mask and prevent deformations of the ultrathin membrane. The submasks were separated from one another by 300 μm to ensure that the diffraction patterns from neighboring slits do not overlap on the detection screen. The average width of the subslits within a given slit varies by less than 1 nm for all slits (SD from the 19 subslits). For submask M_1, the opening width is 86(5) nm. For submask M_2, the opening widths are 75(5) and 81(5) nm with a separation of 102(5) nm. For submask M_3, the opening widths are 79(5) nm and a = 82(5) nm, and their separation is $2d$ = 195(5) nm. For submask M_3, the opening widths are 78(5), 83(5), and 81(5) nm, with separations of 97(5) and 98(5) nm. Here, error bars are the systematic uncertainty of the electron microscope and are consistent with the statistical variations we observed between slits. The 230:1 aspect ratio of the slits and their large opening fraction, a/d = 0.8, helped increase the molecular transmission and therefore signal to noise.

Analysis of diffraction patterns

All four submasks were exposed simultaneously to the molecular beam. However, the limited field of view of the imaging system requires each interference pattern to be imaged separately. To determine κ for a given experimental run, we first centered the individual images $\left[N_1^{(a)}(x,\lambda_{dB}), N_2^{(a,d)}(x,\lambda_{dB}), N_2^{(a,2d)}(x,\lambda_{dB}), N_3^{(a,d)}(x,\lambda_{dB})\right]$ with respect to each other. The horizontal and vertical axes of each image were arranged according to the center of the m = 0 interference fringe, corresponding to x = 0, and the median velocity, respectively. We can align the transverse position of each interference pattern with a precision better than 1 μm in the plane of the detection screen and a vertical precision corresponding to a de Broglie wavelength of 5 fm. Further details are shown in the Supplementary Materials. The molecular velocity for a given vertical pixel was determined from the separation, δx, between the $m = \pm 1$ diffraction orders of the triple-slit diffraction pattern according to $v = 4\pi\hbar L_2/Md\delta x$.

The dark counts per pixel N_0 were subtracted for each interferogram individually. Within a given experimental run, the fractional change in N_0 between different interference patterns is less than 5×10^{-3}. Dark counts were determined by measuring the mean number of counts detected in a square region of 50 pixels × 50 pixels where no molecules are expected. The size and region used to estimate N_0 affect the measurement of $\kappa(x, \lambda_{dB})$ by less than one part in 10^2 when the region of interest is varied between 20 and 200 pixels. This is two orders of magnitude smaller than the statistical uncertainty. The precise position of the same region of interest relative to the center of the interference pattern has a similarly small effect on the measurement of $\kappa(x, \lambda_{dB})$ when the distance is varied between about 700 and 900 pixels.

Surface interactions

Deviations in the slit morphology alter the position-dependent Casimir-Polder interaction between individual molecules and the mask. This has been studied in detail for matter-wave diffraction at material gratings, including the effect of thermally populated rotational and vibrational states on far-field diffraction (*46*, *47*). For each slit, the interference pattern recorded is the ensemble average over the entire phase-space distribution of the molecular beam and the mask. The modification to the interference patterns are therefore negligible for our slits, which are extremely uniform—varying by less than 5 nm from slit to slit. In a previous work by Sinha *et al.* (*35*), the seven different interference patterns necessary to measure $\varepsilon(x, \lambda_{dB})$ were achieved by blocking slits using an additional mask. In our apparatus, this is not possible because of the extremely small opening apertures necessary for our matter waves, which are typically 1000 times smaller than their optical counterparts. In our interferometer, the additional blocking mask would need to be in the vicinity of 100 nm of the diffraction mask, where the strong Casimir interaction between the two masks would modify the transmission function of the unblocked beams. At these short distances, fabrication imperfections in the additional blocking mask would also contribute a systematic distortion of the interference patterns, with a similar magnitude to deviations arising from the diffraction masks themselves.

SUPPLEMENTARY MATERIALS

Supplementary material for this article is available at http://advances.sciencemag.org/cgi/content/full/3/8/e1602478/DC1

Diffraction mask

Molecule detection

Interference patterns

fig. S1. TEM images of the four submasks.

fig. S2. Intensity distribution of the 661-nm illumination light.

fig. S3. Surface migration of PcH_2 molecules behind a grating with a period of 2 μm.

fig. S4. Molecule number as a function of detector position.

fig. S5. Raw data before dark count subtraction.

fig. S6. Determining molecular velocities from fringe spacing.

fig. S7. Reconstructing molecular velocity distributions.

REFERENCES AND NOTES

1. B. J. Bloom, T. L. Nicholson, J. R. Williams, S. L. Campbell, M. Bishof, X. Zhang, W. Zhang, S. L. Bromley, J. Ye, An optical lattice clock with accuracy and stability at the 10^{-18} level. *Nature* **506**, 71–75 (2014).
2. F. Schmidt-Kaler, H. Häffner, M. Riebe, S. Gulde, G. P. T. Lancaster, T. Deuschle, C. Becher, C. F. Roos, J. Eschner, R. Blatt, Realization of the Cirac-Zoller controlled-NOT quantum gate. *Nature* **422**, 408–411 (2003).
3. M. H. Devoret, R. J. Schoelkopf, Superconducting circuits for quantum information: An outlook. *Science* **339**, 1169–1174 (2013).
4. J. R. Maze, P. L. Stanwix, J. S. Hodges, S. Hong, J. M. Taylor, P. Cappellaro, L. Jiang, M. V. G. Dutt, E. Togan, A. S. Zibrov, A. Yacoby, R. L. Walsworth, M. D. Lukin, Nanoscale magnetic sensing with an individual electronic spin in diamond. *Nature* **455**, 644–647 (2008).

5. A. D. Cronin, J. Schmiedmayer, D. E. Pritchard, Optics and interferometry with atoms and molecules. *Rev. Mod. Phys.* **81**, 1051–1129 (2009).
6. G. M. Tino, M. A. Kasevich, Atom interferometry, in *Proceedings of the International School of Physics "Enrico Fermi"* (IOS Press, 2014) chap. 1, pp. 1–87.
7. K. Hornberger, S. Gerlich, P. Haslinger, S. Nimmrichter, M. Arndt, *Colloquium*: Quantum interference of clusters and molecules. *Rev. Mod. Phys.* **84**, 157 (2012).
8. *Many Worlds? Everett, Quantum Theory, and Reality*, S. Saunders, J. Barrett, A. Kent, D. Wallace, Eds. (Oxford Univ. Press, 2010).
9. A. Khrennikov, Towards violation of Born's rule: Description of a simple experiment. *AIP Conf. Proc.* **1327**, 387 (2011).
10. M. F. Pusey, J. Barrett, T. Rudolph, On the reality of the quantum state. *Nat. Phys.* **8**, 475–478 (2012).
11. B. Dakić, T. Paterek, Č. Brukner, Density cubes and higher-order interference theories. *New J. Phys.* **16**, 023028 (2014).
12. M. Ringbauer, B. Duffus, C. Branciard, E. G. Cavalcanti, A. G. White, A. Fedrizzi, Measurements on the reality of the wavefunction. *Nat. Phys.* **11**, 249–254 (2015).
13. D. Nigg, T. Monz, P. Schindler, E. A. Martinez, M. Hennrich, R. Blatt, M. F. Pusey, T. Rudolph, J. Barrett, Can different quantum state vectors correspond to the same physical state? An experimental test. *New J. Phys.* **18**, 013007 (2016).
14. D. Deutsch, Quantum theory of probability and decisions. *Proc. R. Soc. A* **455**, 3129 (1999).
15. W. H. Zurek, Probabilities from entanglement, Born's rule from envariance. *Phys. Rev. A* **71**, 052105 (2005).
16. A. Gleason, Measures on the closed subspaces of a hilbert space. *Indiana Univ. Math. J.* **6**, 885–893 (1957).
17. E. Joos, H. D. Zeh, The emergence of classical properties through interaction with the environment. *Z. Phys. B Con. Mat.* **59**, 223–243 (1985).
18. G. C. Ghirardi, A. Rimini, T. Weber, Unified dynamics for microscopic and macroscopic systems. *Phys. Rev. D* **34**, 470 (1986).
19. T. W. B. Kibble, S. Randjbar-Daemi, Non-linear coupling of quantum theory and classical gravity. *J. Phys. A Math. Gen.* **13**, 141 (1980).
20. L. Diósi, A universal master equation for the gravitational violation of quantum mechanics. *Phys. Lett. A* **120**, 377–381 (1987).
21. W. H. Zurek, Decoherence and the transition from quantum to classical. *Phys. Today* **44**, 36–44 (1991).
22. R. Penrose, On gravity's role in quantum state reduction. *Gen. Relat. Gravit.* **28**, 581–600 (1996).
23. S. L. Adler, A. Bassi, Is quantum theory exact? *Science* **325**, 275–276 (2009).
24. B. Mielnik, Generalized quantum mechanics. *Commun. Math. Phys.* **37**, 221–256 (1974).
25. I. Bialynicki-Birula, J. Mycielski, Nonlinear wave mechanics. *Ann. Phys.* **100**, 62–93 (1976).
26. A. Bassi, K. Lochan, S. Satin, T. P. Singh, H. Ulbricht, Models of wave-function collapse, underlying theories, and experimental tests. *Rev. Mod. Phys.* **85**, 471 (2013).
27. R. Gähler, A. G. Klein, A. Zeilinger, Neutron optical tests of nonlinear wave mechanics. *Phys. Rev. A* **23**, 1611 (1981).
28. C. Curceanu, B. C. Hiesmayr, K. Piscicchia, X-rays help to unfuzzy the concept of measurement. *J. Adv. Phys.* **4**, 263–266 (2015).
29. M. Arndt, K. Hornberger, Testing the limits of quantum mechanical superpositions. *Nat. Phys.* **10**, 271–277 (2014).
30. A. D. O'Connell, M. Hofheinz, M. Ansmann, R. C. Bialczak, M. Lenander, E. Lucero, M. Neeley, D. Sank, H. Wang, M. Weides, J. Wenner, J. M. Martinis, A. N. Cleland, Quantum ground state and single-phonon control of a mechanical resonator. *Nature* **464**, 697–703 (2010).
31. J. Chan, T. P. M. Alegre, A. H. Safavi-Naeini, J. T. Hill, A. Krause, S. Gröblacher, M. Aspelmeyer, O. Painter, Laser cooling of a nanomechanical oscillator into its quantum ground state. *Nature* **478**, 89–92 (2011).
32. S. Eibenberger, S. Gerlich, M. Arndt, M. Mayor, J. Tüxen, Matter-wave interference of particles selected from a molecular library with masses exceeding 10 000 amu. *Phys. Chem. Chem. Phys.* **15**, 14696–14700 (2013).
33. T. Kovachy, P. Asenbaum, C. Overstreet, C. A. Donnelly, S. M. Dickerson, A. Sugarbaker, J. M. Hogan, M. A. Kasevich, Quantum superposition at the half-metre scale. *Nature* **528**, 530–533 (2015).
34. R. D. Sorkin, Quantum mechanics as quantum measure theory. *Mod. Phys. Lett. A* **9**, 3119 (1994).
35. U. Sinha, C. Couteau, T. Jennewein, R. Laflamme, G. Weihs, Ruling out multi-order interference in quantum mechanics. *Science* **329**, 418–421 (2010).
36. I. Söllner, B. Gschösser, P. Mai, B. Pressl, Z. Vörös, G. Weihs, Testing Born's rule in quantum mechanics for three mutually exclusive events. *Found. Phys.* **42**, 742–751 (2012).
37. T. Kauten, R. Keil, T. Kaufmann, B. Pressl, Č. Brukner, G. Weihs, Obtaining tight bounds on higher-order interferences with a 5-path interferometer. *New J. Phys.* **19**, 033017 (2017).
38. O. S. Magaña-Loaiza, I. De Leon, M. Mirhosseini, R. Fickler, A. Safari, U. Mick, B. McIntyre, P. Banzer, B. Rodenburg, G. Leuchs, R. W. Boyd, Exotic looped trajectories of photons in three-slit interference. *Nat. Commun.* **7**, 13987 (2016).
39. J. M. Hickmann, E. J. S. Fonseca, A. J. Jesus-Silva, Born's rule and the interference of photons with orbital angular momentum by a triangular slit. *EPL* **96**, 64006 (2011).
40. D. K. Park, O. Moussa, R. Laflamme, Three path interference using nuclear magnetic resonance: A test of the consistency of Born's rule. *New J. Phys.* **14**, 113025 (2012).
41. T. Juffmann, A. Milic, M. Müllneritsch, P. Asenbaum, A. Tsukernik, J. Tüxen, M. Mayor, O. Cheshnovsky, M. Arndt, Real-time single-molecule imaging of quantum interference. *Nat. Nanotechnol.* **7**, 297–300 (2012).
42. M. Arndt, K. Hornberger, A. Zeilinger, Probing the limits of the quantum world. *Phys. World* **18**, 35 (2005).
43. C. Brand, M. Sclafani, C. Knobloch, Y. Lilach, T. Juffmann, J. Kotakoski, C. Mangler, A. Winter, A. Turchanin, J. Meyer, O. Cheshnovsky, M. Arndt, An atomically thin matter-wave beamsplitter. *Nat. Nanotechnol.* **10**, 845–848 (2015).
44. A. Sinha, A. H. Vijay, U. Sinha, On the superposition principle in interference experiments. *Sci. Rep.* **5**, 10304 (2015).
45. G. Rengaraj, U. Prathwiraj, S. N. Sahoo, R. Somashekhar, U. Sinha, Measuring the deviation from the superposition principle in interference experiments. arXiv:1610.09143 (2016).
46. C. Brand, J. Fiedler, T. Juffmann, M. Sclafani, C. Knobloch, S. Scheel, Y. Lilach, O. Cheshnovsky, M. Arndt, A Green's function approach to modeling molecular diffraction in the limit of ultra-thin gratings. *Ann. Phys.* **527**, 580–591 (2015).
47. J. Fiedler, S. Scheel, Casimir-Polder potentials on extended molecules. *Ann. Phys.* **527**, 570–579 (2015).

Acknowledgments: We thank B. Dakic and C. Brukner for helpful discussions and T. Susi for help with the recording of TEM images. **Funding:** We are grateful for financial support from the Austrian Science Fund (FWF) (W1210-3), the European Research Council (320694), and the European Commission (304886). J.P.C. is supported by a Vienna Center for Quantum Science and Technology fellowship. C.B. acknowledges support from the Alexander von Humboldt-Foundation through a Feodor-Lynen fellowship. **Author contributions:** J.P.C. and M.A. devised the experiment. Y.L. and O.C. prepared the diffraction mask. C.B. and C.K. acquired the data. J.P.C. analyzed the data. All authors discussed the results and contributed to the writing of the paper. **Competing interests:** The authors declare that they have no competing interests. **Data and materials availability:** All data needed to evaluate the conclusions in the paper are present in the paper and/or the Supplementary Materials. Additional data related to this paper may be requested from J.P.C. (joseph.cotter@univie.ac.at).

Submitted 12 October 2016
Accepted 6 July 2017
Published 11 August 2017
10.1126/sciadv.1602478

Citation: J. P. Cotter, C. Brand, C. Knobloch, Y. Lilach, O. Cheshnovsky, M. Arndt, In search of multipath interference using large molecules. *Sci. Adv.* **3**, e1602478 (2017).

In search of multipath interference using large molecules

Joseph P. Cotter, Christian Brand, Christian Knobloch, Yigal Lilach, Ori Cheshnovsky and Markus Arndt

Sci Adv **3** (8), e1602478.
DOI: 10.1126/sciadv.1602478